Results in Physics 8 (2018) 489–495

Contents lists available at ScienceDirect

Results in Physics

journal homepage: www.journals.elsevier.com/results-in-physics

Cattaneo-Christov double-diffusion theory for three-dimensional flow of viscoelastic nanofluid with the effect of heat generation/absorption

Tasawar Hayat [a,b], Sajid Qayyum [a,*], Sabir Ali Shehzad [c], Ahmed Alsaedi [b]

[a] Department of Mathematics, Quaid-I-Azam University, 45320 Islamabad 44000, Pakistan
[b] Nonlinear Analysis and Applied Mathematics (NAAM) Research Group, Faculty of Science, King Abdulaziz University, P.O. Box 80207, Jeddah 21589, Saudi Arabia
[c] Department of Mathematics, COMSATS Institute of Information Technology, Sahiwal 57000, Pakistan

ARTICLE INFO

Article history:
Received 15 November 2017
Received in revised form 21 December 2017
Accepted 22 December 2017
Available online 27 December 2017

Keywords:
Viscoelastic(second grade) nanofluid
Cattaneo-Christov double-diffusion model
Heat generation/absorption

ABSTRACT

The present research article focuses on three-dimensional flow of viscoelastic(second grade) nanofluid in the presence of Cattaneo-Christov double-diffusion theory. Flow caused is due to stretching sheet. Characteristics of heat transfer are interpreted by considering the heat generation/absorption. Nanofluid theory comprises of Brownian motion and thermophoresis. Cattaneo-Christov double-diffusion theory is introduced in the energy and concentration expressions. Such diffusions are developed as a part of formulating the thermal and solutal relaxation times framework. Suitable variables are implemented for the conversion of partial differential systems into a sets of ordinary differential equations. The transformed expressions have been explored through homotopic algorithm. Behavior of sundry variables on the velocities, temperature and concentration are scrutinized graphically. Numerical values of skin friction coefficients are also calculated and examined. Here thermal field enhances for heat generation parameter while reverse situation is noticed for heat absorption parameter.

Introduction

The dilute suspension of nano-sized particles and dispersion of fibers in a fluid is termed as nanoliquid. The mixture of nanoparticles changed the physical nature of liquid in comparison to ordinary fluids e.g. density, thermal conductivity, viscosity etc. In all such characteristics, thermal conductivity has role in various industrial and technological applications. The nanoparticles are widely implemented in the applications of medicine, electronics, optics, solar cells, catalysis, materials, manufacturing, smart computers, renewable energy and many others. At present the concept of energy transfer in nanoliquids can be categorized in two classes. In one category, the researchers assumed that the nanoliquids are composite, developed by nanoparticles and surrounded by nanolayers like shell. Some investigations on this concept can be found in the studies [1–10]. The other theory states that the thermal conductivity of nanoliquid based on part of Brownian motion and particle convention static due to which micro-mixing occurs. The dynamics of particles is considered in such models. The interaction of particle mechanism in nanoliquids can be visualized through this theory. Buongiorno [11] developed a model to explore the mechanism of thermal conductivity of nanoliquids by considering the Brownian motion and thermophoretic. Further researches on this topic can be seen in the studies [12–18].

In the past, the investigators made the analysis of heat and mass transport problems by employing classical Fourier and Fick's theories of heat and mass diffusion. In these theories, the anomalous of heat and mass diffusion is ignored. Cattaneo [19] firstly proposed the concept of thermal relaxation time in Fourier's theory of heat transport to denote the "thermal inertia". This idea is known as Maxwell–Cattaneo theory of heat flux. Christov [20] used the upper-convective Oldroyd differentiation in place of partial time derivative and he also employed the frame indifferent generalization of Fourier's law in energy expression [21]. Haddad [22] explored the thermal instability Cattaneo-Christov formula of heat flux in a non-Darcy porous space. Li et al. [23] extended the concept of Cattaneo-Christov for hydromagnetic flow of Maxwell liquid induced by a vertical moving surface. The aspects of Cattaneo-Christov double-diffusion model for flow of Jeffrey fluid over a stretched are reported by Hayat et al. [24]. Waqas et al. [25] explored the impact of thermal relaxation time for variable conductivity flow of non-Newtonian fluid. They employed the homotopic theory to evaluate the results of governing model. Shehzad et al. [26] addressed the Oldroyd-B liquid flow in a Darcy-Forchheimer porous media through Cattaneo-Christov heat diffusion. Sui et al. [27] examined the double-diffusive model of Cattaneo-Christov for Maxwell liquid flow with Brownian motion

* Corresponding author.
E-mail address: sajid@math.qau.edu.pk (S. Qayyum).

https://doi.org/10.1016/j.rinp.2017.12.060
2211-3797/

and slip conditions. Hayat et al. [28] discussed the squeezed flow of Jeffrey fluid in the frame of Cattaneo-Christov heat flux.

The main idea here is to evaluate impact of Cattaneo-Christov heat and mass diffusions model for flow of second grade liquid. Second grade model is an important sub-category of non-Newtonian liquids. Such liquids have vital roles in the applications like movement of biological liquids, lubricants performance, plastic manufacturing, food processing etc. Aspects of Brownian motion, thermophoretic and heat absorption/generation are further considered in this work. The theory of boundary layer is employed to govern the mathematical expressions of considered flow model. Computations of solutions are made through homotopic theory [29–46]. The results of presented analysis are displayed and discussed.

Formulation

We investigate three-dimensional flow of an incompressible viscoelastic nanofluid over a impermeable stretching surface at $z=0$. The flow is confined in the domain $z>0$. Here we choose the Cartesian coordinate in such away that x-axis is along the stretching sheet and y-axis perpendicular to sheet (see Fig. 1). Let (u,v,w) be the velocity components along the (x,y,z) directions, respectively. Here $u_w(x)=ax$ and $v_w(y)=by$ are stretching velocity components (where a and b being stretching rate constants having dimension T^{-1}). The heat and nanoparticle mass transfer phenomena have been analyzed in view of Cattaneo-Christov double-diffusion expressions. The behavior of thermophoresis and Brownian motion is taken into account. The equations are

$$\frac{\partial u}{\partial x}+\frac{\partial v}{\partial y}+\frac{\partial w}{\partial z}=0, \tag{1}$$

$$u\frac{\partial u}{\partial x}+v\frac{\partial u}{\partial y}+w\frac{\partial u}{\partial z}=\nu\frac{\partial^2 u}{\partial z^2} +\beta\left[u\frac{\partial^3 u}{\partial x\partial z^2}+w\frac{\partial^3 u}{\partial z^3}-\frac{\partial u}{\partial x}\frac{\partial^2 u}{\partial z^2}-\frac{\partial u}{\partial z}\frac{\partial^2 w}{\partial z^2}-2\frac{\partial u}{\partial z}\frac{\partial^2 u}{\partial x\partial z}-2\frac{\partial w}{\partial z}\frac{\partial^2 u}{\partial^2 z}\right], \tag{2}$$

$$u\frac{\partial v}{\partial x}+v\frac{\partial v}{\partial y}+w\frac{\partial v}{\partial z}=\nu\frac{\partial^2 v}{\partial z^2} +\beta\left[v\frac{\partial^3 v}{\partial x\partial z^2}+w\frac{\partial^3 v}{\partial z^3}-\frac{\partial v}{\partial y}\frac{\partial^2 v}{\partial z^2}-\frac{\partial v}{\partial z}\frac{\partial^2 w}{\partial z^2}-2\frac{\partial v}{\partial z}\frac{\partial^2 v}{\partial y\partial z}-2\frac{\partial w}{\partial z}\frac{\partial^2 v}{\partial^2 z}\right], \tag{3}$$

with the boundary conditions

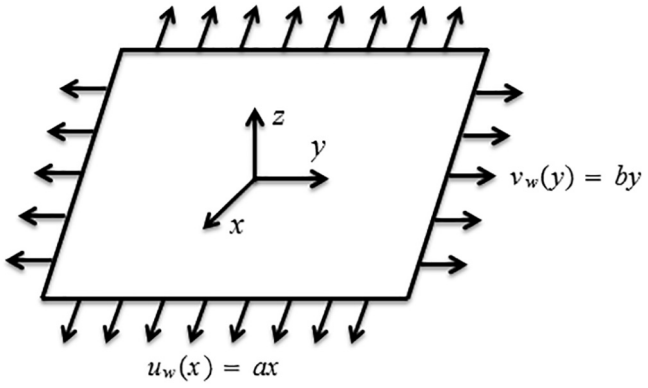

Fig. 1. Physical sketch.

$$u=u_w(x)=ax,\ v=v_w(y)=by,\ w=0 \text{ at } z=0,\quad u\to 0,\ v\to 0 \text{ as } y\to\infty, \tag{4}$$

where $\nu=(\mu/\rho)_f$ denotes the kinematic viscosity, β for normal stress moduli and ρ_f for viscoelastic fluid density. The Cattaneo-Christov diffusion theory describing the thermal and concentration diffusion with relaxation of heat and mass fluxes are

$$\mathbf{q}+\Lambda_e\left[\frac{\partial \mathbf{q}}{\partial t}+\mathbf{V}\cdot\nabla\mathbf{q}-\mathbf{q}\cdot\nabla\mathbf{V}+(\nabla\cdot\mathbf{V})\mathbf{q}\right]=-k_f\nabla T, \tag{5}$$

$$\mathbf{J}+\Lambda_c\left[\frac{\partial \mathbf{J}}{\partial t}+\mathbf{V}\cdot\nabla\mathbf{J}-\mathbf{J}\cdot\nabla\mathbf{V}+(\nabla\cdot\mathbf{V})\mathbf{J}\right]=-D_B\nabla C, \tag{6}$$

where $\mathbf{q}$ is for heat flux and $\mathbf{J}$ for mass flux, $\mathbf{V}$ for velocity, k_f for fluid thermal conductivity and D_B for Brownian diffusion coefficient. Here Λ_e and Λ_c are the thermal and solutal relaxation time factors. For $\Lambda_e=0$ and $\Lambda_c=0$, the Eqs. (5) and (6) recovers laws due to Fourier and Fick. For incompressible fluid situation one has

$$\mathbf{q}+\Lambda_e[\mathbf{V}\cdot\nabla\mathbf{q}-\mathbf{q}\cdot\nabla\mathbf{V}]=-k_f\nabla T, \tag{7}$$

$$\mathbf{J}+\Lambda_c[\mathbf{V}\cdot\nabla\mathbf{J}-\mathbf{J}\cdot\nabla\mathbf{V}]=-D_B\nabla C. \tag{8}$$

The energy and concentration expressions are

$$u\frac{\partial T}{\partial x}+v\frac{\partial T}{\partial y}+w\frac{\partial T}{\partial z}+\Omega_e\Lambda_e=\frac{k_f}{(\rho c_p)_f}\frac{\partial^2 T}{\partial z^2}+\tau D_B\left(\frac{\partial T}{\partial z}\frac{\partial C}{\partial z}\right) +\frac{\tau D_T}{T_\infty}\left(\frac{\partial T}{\partial z}\right)^2+\frac{Q^*}{(\rho c_p)_f}(T-T_\infty), \tag{9}$$

$$u\frac{\partial C}{\partial x}+v\frac{\partial C}{\partial y}+w\frac{\partial C}{\partial z}+\Omega_c\Lambda_c=D_B\frac{\partial^2 C}{\partial z^2}+\frac{D_T}{T_\infty}\left(\frac{\partial^2 T}{\partial z^2}\right), \tag{10}$$

with

$$T=T_w,\ C=C_w \text{ at } z=0 \text{ and } T\to T_\infty,\ C\to C_\infty \text{ as } z\to\infty, \tag{11}$$

$$\Omega_e=u^2\frac{\partial^2 T}{\partial x^2}+v^2\frac{\partial^2 T}{\partial y^2}+w^2\frac{\partial^2 T}{\partial z^2}+\left(u\frac{\partial u}{\partial x}+v\frac{\partial u}{\partial y}+w\frac{\partial u}{\partial z}\right)\frac{\partial T}{\partial x} +\left(u\frac{\partial v}{\partial x}+v\frac{\partial v}{\partial y}+w\frac{\partial v}{\partial z}\right)\frac{\partial T}{\partial y}+\left(u\frac{\partial w}{\partial x}+v\frac{\partial w}{\partial y}+w\frac{\partial w}{\partial z}\right)\frac{\partial T}{\partial z} +2uv\frac{\partial^2 T}{\partial x\partial y}+2vw\frac{\partial^2 T}{\partial y\partial z}+2uw\frac{\partial^2 T}{\partial x\partial z}, \tag{12}$$

$$\Omega_c=u^2\frac{\partial^2 C}{\partial x^2}+v^2\frac{\partial^2 C}{\partial y^2}+w^2\frac{\partial^2 C}{\partial z^2}+\left(u\frac{\partial u}{\partial x}+v\frac{\partial u}{\partial y}+w\frac{\partial u}{\partial z}\right)\frac{\partial C}{\partial x} +\left(u\frac{\partial v}{\partial x}+v\frac{\partial v}{\partial y}+w\frac{\partial v}{\partial z}\right)\frac{\partial C}{\partial y}+\left(u\frac{\partial w}{\partial x}+v\frac{\partial w}{\partial y}+w\frac{\partial w}{\partial z}\right)\frac{\partial C}{\partial z} +2uv\frac{\partial^2 C}{\partial x\partial y}+2vw\frac{\partial^2 C}{\partial y\partial z}+2uw\frac{\partial^2 C}{\partial x\partial z}. \tag{13}$$

In the above expressions ρ_f for fluid density, $(c_p)_f$ for fluid heat capacity, ρ_p for particle density, $(c_p)_p$ for particle heat capacity, k_f for thermal conductivity, $\tau=(\rho c_p)_p/(\rho c_p)_f$ for heat capacity ratio, D_B for Brownian diffusion coefficient, D_T for thermophoretic diffusion coefficient, Q^* for coefficient of heat generation/absorption, T and C for temperature and nanoparticle concentration of fluid respectively, T_w and C_w for temperature and nanoparticle concentration of surface respectively, T_∞ for ambient fluid temperature and C_∞ for ambient fluid concentration. The suitable transformations are

$$\eta=z\sqrt{\frac{a}{\nu}},\ \theta(\eta)=\frac{T-T_\infty}{T_w-T_\infty},\ \phi(\eta)=\frac{C-C_\infty}{C_w-C_\infty},\quad u=axf'(\eta),\ v=ayg'(\eta),\ w=-\sqrt{a\nu}(f(\eta)+g(\eta)). \tag{14}$$

Eq. (1) is trivially satisfied by variables defined in previous equation and other equations yield

$$f''' + (f+g)f'' - (f')^2 + \alpha\left((f+g)f^{iv} + (f''-g'')f'' - 2(f'+g')f'''\right) = 0, \tag{15}$$

$$g''' + (f+g)g'' - (g')^2 + \alpha\left((f+g)g^{iv} + (f''-g'')g'' - 2(f'+g')g'''\right) = 0, \tag{16}$$

$$\theta'' + \Pr(f+g)\theta' - \Pr\delta_e\left((f+g)^2\theta'' + (f+g)(f'+g')\theta'\right) + \Pr N_b\theta'\phi' + \Pr N_t(\theta')^2 + \Pr\gamma\theta = 0, \tag{17}$$

$$\phi'' + Sc(f+g)\phi' - Sc\delta_c\left((f+g)^2\phi'' + (f+g)(f'+g')\phi'\right) + \frac{N_t}{N_b}\theta'' = 0, \tag{18}$$

$$f(\eta)=0, f'(\eta)=1, g(\eta)=0, g'(\eta)=\delta, \theta(\eta)=1, \phi(\eta)=1 \text{ at } \eta=0,$$
$$f'(\eta)\to 0, g(\eta)\to 0, \theta(\eta)\to 0, \phi(\eta)\to 0 \text{ as } \eta\to\infty, \tag{19}$$

where α for dimensionless viscoelastic parameter, Pr for Prandtl number, N_b for Brownian motion parameter, N_t for thermophoresis parameter, γ for heat generation/absorption parameter, δ_e for non-dimensional thermal relaxation time, Sc for Schmidt number, δ_c for non-dimensional solutal relaxation time and $\delta$for ratio parameter. The involved variables are defined as:

$$\alpha=\frac{\beta a}{\nu}, \Pr=\frac{\mu c_p}{k_f}, N_b=\frac{(\rho c_p)_p D_B(C_w-C_\infty)}{(\rho c_p)_f \nu}, N_t=\frac{(\rho c_p)_p D_T(T_w-T_\infty)}{(\rho c_p)_f \nu T_\infty},$$
$$\gamma=\frac{Q^*}{(\rho c_p)_f a}, \delta_e=\Lambda_e a, Sc=\frac{\nu}{D_B}, \delta_c=\Lambda_c a, \delta=\frac{b}{a}. \tag{20}$$

It should be noted that $g(\eta)=\delta=0$ in Eqs. (15)–(19) yields two-dimensional situation.

The skin friction coefficient along the x and y directions are defined for the given problem in the forms

$$C_{f_x}=\frac{\tau_{wx}}{\frac{1}{2}\rho u_w^2}, \quad C_{f_y}=\frac{\tau_{wy}}{\frac{1}{2}\rho u_w^2}, \tag{21}$$

where τ_{wx} and τ_{wy} denote the surface shear stresses along the x and y directions which can be expressed as

$$\tau_{wx}=\left[\mu\frac{\partial u}{\partial z}+\beta\left(u\frac{\partial^2 u}{\partial x\partial z}+v\frac{\partial^2 u}{\partial y\partial z}+w\frac{\partial^2 u}{\partial z^2}+\frac{\partial u}{\partial x}\frac{\partial u}{\partial z}+\frac{\partial v}{\partial x}\frac{\partial v}{\partial z}-\frac{\partial w}{\partial z}\frac{\partial u}{\partial z}\right)\right]_{z=0},$$
$$\tau_{wy}=\left[\mu\frac{\partial v}{\partial z}+\beta\left(u\frac{\partial^2 v}{\partial x\partial z}+v\frac{\partial^2 v}{\partial y\partial z}+w\frac{\partial^2 v}{\partial z^2}+\frac{\partial u}{\partial y}\frac{\partial u}{\partial z}+\frac{\partial v}{\partial y}\frac{\partial v}{\partial z}-\frac{\partial w}{\partial z}\frac{\partial v}{\partial z}\right)\right]_{z=0} \tag{22}$$

In dimensionless form the skin friction coefficients C_{f_x} and C_{f_y} along x and y directions are given by

$$\frac{1}{2}\mathrm{Re}_x^{0.5}C_{f_x}=\left[f''+\alpha\left(-(f+g)f'''+2f'f''+(f'+g')f''\right)\right]_{\eta=0},$$
$$\frac{1}{2}\mathrm{Re}_y^{0.5}C_{f_y}=\left[g''+\alpha\left(-(f+g)g'''+2g'g''+(f'+g')g''\right)\right]_{\eta=0}, \tag{23}$$

in which $\mathrm{Re}_x=\frac{u_w x}{\nu}$ and $\mathrm{Re}_y=\frac{u_w y}{\nu}$ denote the local Reynolds number.

Solutions expressions

The initial approximations $(f_0, g_0, \theta_0, \phi_0)$ and auxiliary linear operators $(\mathcal{L}_f, \mathcal{L}_g, \mathcal{L}_\theta, \mathcal{L}_\phi)$ for homotopic expressions are

$$f_0(\eta)=(1-\exp(-\eta)), \ g_0(\eta)=\delta(1-\exp(-\eta)),$$
$$\theta_0(\eta)=\exp(-\eta), \ \phi_0(\eta)=\exp(-\eta), \tag{24}$$

$$_f(f)=\frac{d^3 f}{d\eta^3}-\frac{df}{d\eta}, \ \mathcal{L}_g(g)=\frac{d^3 g}{d\eta^3}-\frac{dg}{d\eta},$$
$$\mathcal{L}_\theta(\theta)=\frac{d^2\theta}{d\eta^2}-\theta, \ \mathcal{L}_\phi(\phi)=\frac{d^2\phi}{d\eta^2}-\phi, \tag{25}$$

with the associated properties

$$\mathcal{L}_f[\Gamma_1+\Gamma_2\exp(-\eta)+\Gamma_3\exp(\eta)]=0,$$
$$\mathcal{L}_g[\Gamma_4+\Gamma_5\exp(-\eta)+\Gamma_6\exp(\eta)]=0,$$
$$\mathcal{L}_\theta[\Gamma_7\exp(-\eta)+\Gamma_8\exp(\eta)]=0,$$
$$\mathcal{L}_\phi[\Gamma_9\exp(-\eta)+\Gamma_{10}\exp(\eta)]=0. \tag{26}$$

Employing procedure in Refs. [43–46] we have the general solutions

$$f_m(\eta)=f_m^*(\eta)+\Gamma_1+\Gamma_2\exp(-\eta)+\Gamma_3\exp(\eta),$$
$$g_m(\eta)=g_m^*(\eta)+\Gamma_4+\Gamma_5\exp(-\eta)+\Gamma_6\exp(\eta),$$
$$\theta_m(\eta)=\theta_m^*(\eta)+\Gamma_7\exp(-\eta)+\Gamma_8\exp(\eta),$$
$$\phi_m(\eta)=\phi_m^*(\eta)+\Gamma_9\exp(-\eta)+\Gamma_{10}\exp(\eta), \tag{27}$$

where $f_m^*(\eta), g_m^*(\eta), \theta_m^*(\eta)$ and $\phi_m^*(\eta)$ are the special solutions and Γ_i $(i=1-10)$ are the arbitrary constants given by

$$\Gamma_1=-\left.\frac{\partial f_m^*(\eta)}{\partial\eta}\right|_{\eta=0}-f_m^*(0), \ \Gamma_2=\left.\frac{\partial f_m^*(\eta)}{\partial\eta}\right|_{\eta=0}, \ \Gamma_3=0,$$
$$\Gamma_4=-\left.\frac{\partial g_m^*(\eta)}{\partial\eta}\right|_{\eta=0}-g_m^*(0), \ \Gamma_5=\left.\frac{\partial g_m^*(\eta)}{\partial\eta}\right|_{\eta=0}, \ \Gamma_6=0,$$
$$\Gamma_7=-\left.\theta_m^*(\eta)\right|_{\eta=0}, \ \Gamma_8=0, \ \Gamma_9=-\left.\phi_m^*(\eta)\right|_{\eta=0}, \ \Gamma_{10}=0. \tag{28}$$

Convergence analysis

Construction of the series solutions by homotopy analysis technique involve convergence control variables $\hbar_f, \hbar_g, \hbar_\theta$ and $\hbar_\phi$. These convergence control variables plays vital role to adjust and control the convergence region of the series solutions. Hence Figs. 2 and 3 displayed the $\hbar$-curves. It is seen that acceptable values of $\hbar_f, \hbar_g, \hbar_\theta$ and $\hbar_\phi$ are $-2.1\leqslant\hbar_f\leqslant-0.15, -2.1\leqslant\hbar_g\leqslant-0.25, -1.3\leqslant\hbar_\theta\leqslant-0.2$ and $-1.2\leqslant\hbar_\phi\leqslant-0.25$.

Results and discussion

The effect of various physical variables on the velocities, thermal and concentration fields are interpreted in this section. Figs. 4 and 5 ensure the impact of dimensionless viscoelastic parameter α and ratio parameter δon velocities $f'(\eta)$ and $g'(\eta)$. Variation of velocities of $f'(\eta)$ and $g'(\eta)$ within the frame of viscoelastic param-

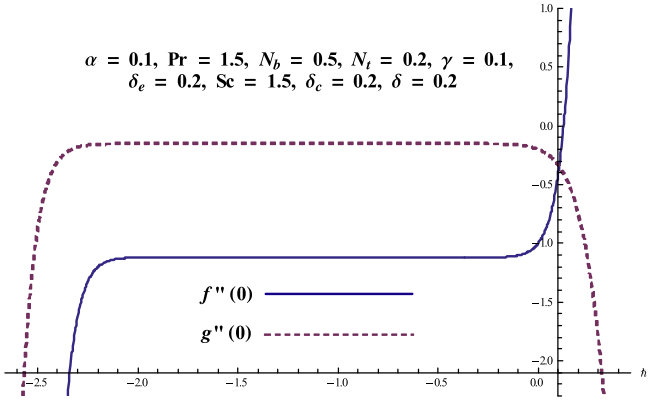

Fig. 2. $\hbar$-curves for $f''(0)$ and $g''(0)$.

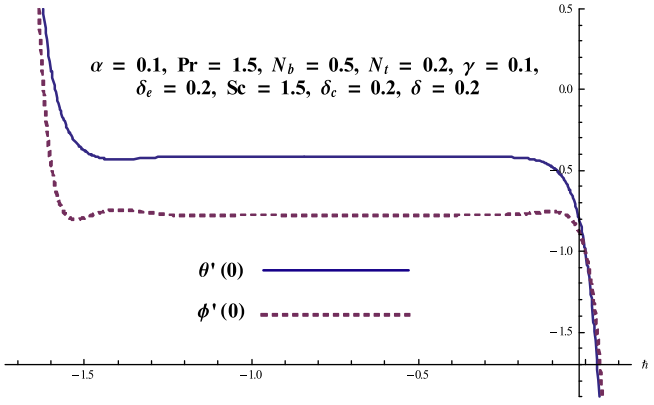

Fig. 3. $\hbar$-curves for $\theta'(0)$ and $\phi'(0)$.

eter α are captured in Fig. 4. One can see that velocities and layer thickness are reduced via larger α. Physically it can be observed that for higher values of α, the viscoelasticity enhances which resists the fluid flow due to which the fluid velocities are diminished. Fig. 5 illustrates the behavior of δ on x- and y-components of velocity. Large δ implies to an increase in rate of stretching along y-direction due to which velocity field $g'(\eta)$ is increasing whereas $f'(\eta)$ shows the decreasing behavior.

Variations in temperature for different values of viscoelastic parameter α, Prandtl number Pr, Brownian motion parameter N_b, thermophoresis parameter N_t, heat generation/absorption parameter γ and non-dimensional thermal relaxation time δ_e are studied in the Figs. 6–11. Fig. 6 disclosed the behavior of α on the temperature. Both temperature and thermal layer thickness are enhanced via α. Physically larger viscoelastic parameter result in more temperature inside the boundary layer region. It is seen from Fig. 7 that both temperature and thickness layer diminish for higher Prandtl number Pr. Physically, higher Pr lead to lower thermal diffusivity which ensures decrease in temperature. Fig. 8 demonstrates the features of Brownian motion parameter N_b on temperature field. There is an enhancement in temperature and thermal layer thickness in view of N_b. In fact more heat is produced through the random motion of the fluid particles within the frame of larger Brownian motion parameter N_b. Therefore temperature increases. Fig. 9 clearly indicates that the temperature and associated layer thickness are increased for larger thermophoresis parameter N_t. In thermophoresis phenomenon the heated particles are pulled away from hot surface to the cold region and fluid temperature rises. Behavior of heat generation/absorption parameter γ on temperature field is elucidated in Fig. 10. It is concluded that temperature and thickness of thermal layer are enhanced when heat generation parameter ($\gamma > 0$) increases while reverse situation is observed for heat absorption situation ($\gamma < 0$). Obviously in heat generation parameter $\gamma > 0$ process more heat is produced which results in the enhancement of temperature field. Variation of temperature field within the frame of non-dimensional thermal relaxation time δ_e is shown in Fig. 11. One can see that temperature and thermal layer thickness are reduced via larger δ_e. Physically it

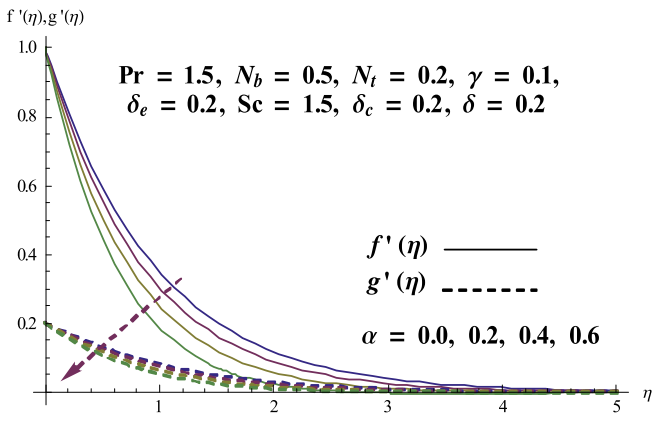

Fig. 4. Behavior of α on $f'(\eta)$.

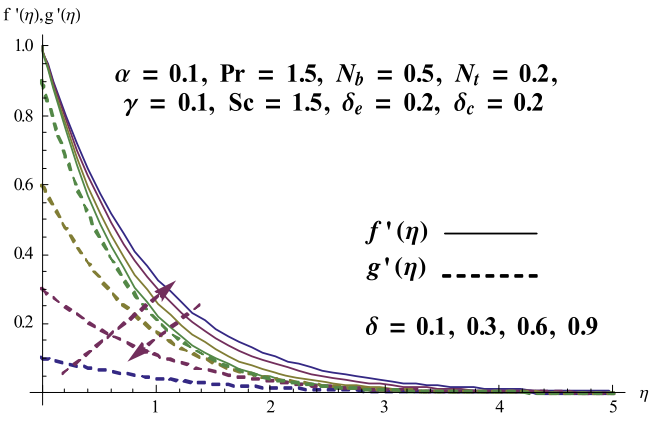

Fig. 5. Behavior of δ on $f'(\eta)$.

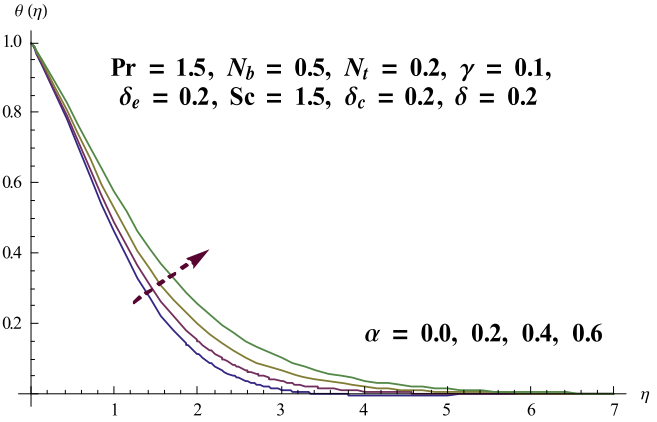

Fig. 6. Behavior of α on $\theta(\eta)$.

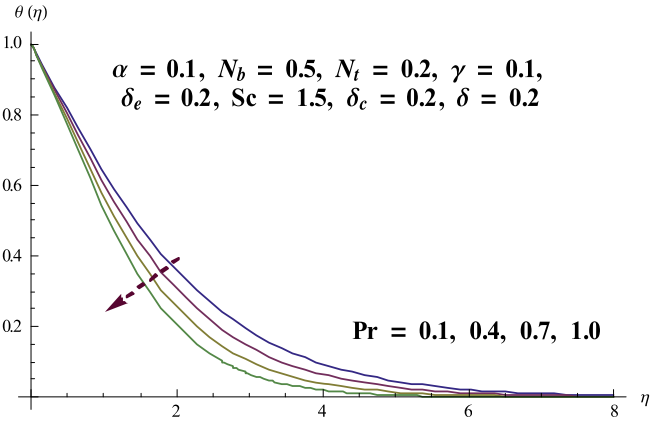

Fig. 7. Behavior of Pr on $\theta(\eta)$.

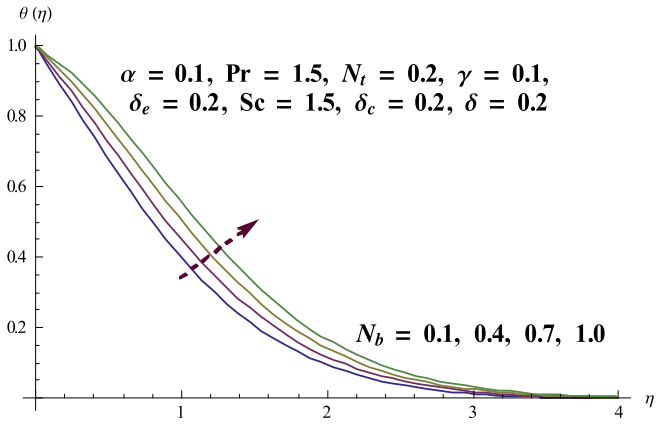

Fig. 8. Behavior of N_b on $\theta(\eta)$.

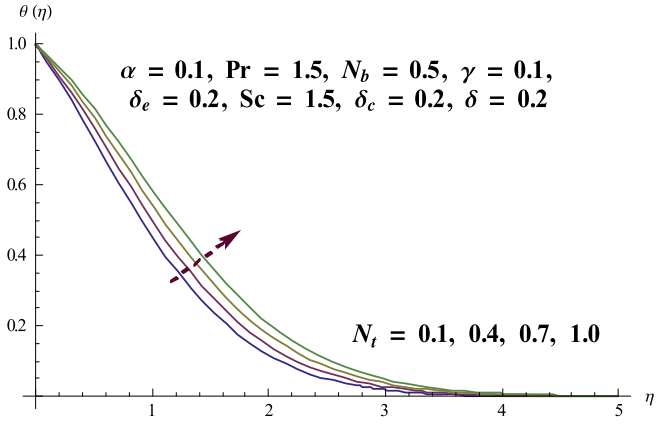

Fig. 9. Behavior of N_t on $\theta(\eta)$.

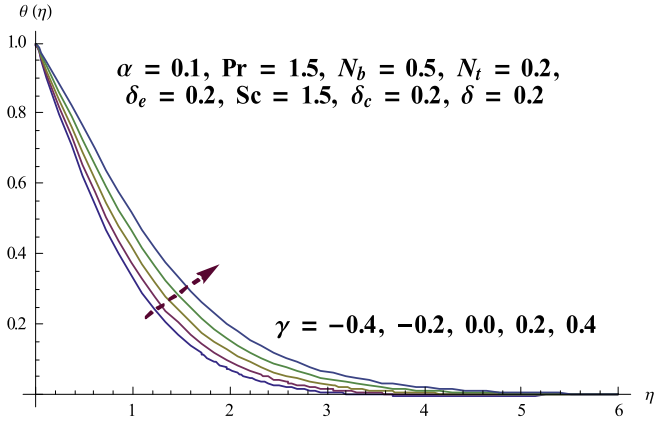

Fig. 10. Behavior of γ on $\theta(\eta)$.

can be observed that material particle requires more time for heat transfer to its neighboring particles due to thermal relaxation enhancement.

Influences of dimensionless viscoelastic parameter α, Brownian motion parameter N_b, thermophoresis parameter N_t, Schmidt number Sc and non-dimensional solutal relaxation time δ_c on the nanoparticle concentration are analyzed in the Figs. 12–16. Fig. 12 is prepared to see the behavior of viscoelastic parameter α on concentration field. We see that both concentration and

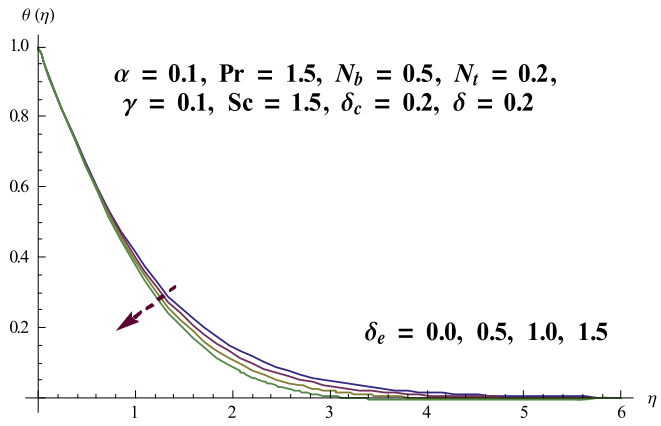

Fig. 11. Behavior of δ_e on $\theta(\eta)$.

boundary layer thickness are increasing via α. Fig. 13 exhibits impact of Brownian motion parameter N_b on the concentration distribution. For higher values of N_b the concentration and layer thickness have dominant behavior. It is interpreted that for larger Brownian motion parameter N_b,the collision of the fluid particles enhances and the concentration field diminishes. Fig. 14 shows that both concentration profile and boundary layer thickness are enhanced for larger thermophoresis parameter N_t. The thermal conductivity of the fluid enhances in presence of nanoparticles. Higher N_t give rise to thermal conductivity of the fluid. Such higher thermal conductivity indicates rise in concentration. It is revealed that concentration and related layer thickness are reduced for larger Schmidt number Sc (see Fig. 15). Physically Schmidt number Sc is the momentum to mass diffusivities ratio. Thus for larger Schmidt number Sc the mass diffusivity decreases which is responsible in reduction of concentration field. Fig. 16 presents impact of non-dimensional solutal relaxation time δ_c on concentration distribution. Through δ_c the concentration and layer thickness are diminished. In fact that material particle requires more time for mass transfer to its neighboring particles due to solutal relaxation enhancement.

Table 1 explores the convergence of velocities $f'(\eta)$ and $g'(\eta)$, temperature and concentration. Presented values scrutinized that 16th order of approximations are enough for $f''(0)$ and $g''(0)$ and 8th and 20th orders of approximations are sufficient for $\theta'(0)$ and $\phi'(0)$. Table 2 computed skin friction coefficients for various values

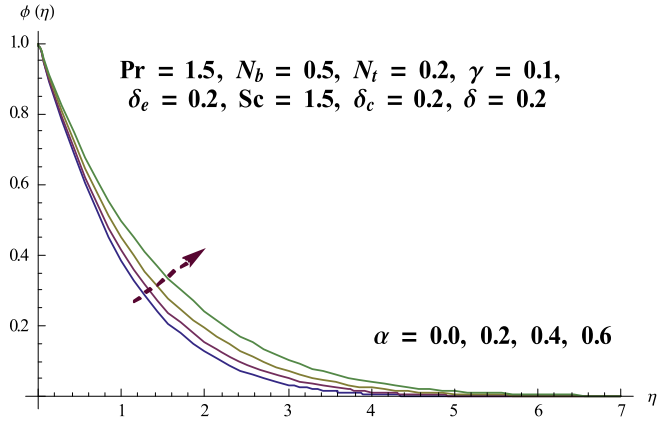

Fig. 12. Behavior of α on $\phi(\eta)$.

Table 1
Convergence solutions when $\alpha = 0.1, \Pr = 1.5, N_b = 0.5, N_t = 0.2, \gamma = 0.1, \delta_e = 0.2, Sc = 1.5, \delta_c = 0.2$ and $\delta = 0.2$.

Order of approximation	$-f''(0)$	$-g''(0)$	$-\theta'(0)$	$-\phi'(0)$
1	1.05333	0.18400	0.62500	0.92000
5	1.11434	0.15784	0.42485	0.82930
8	1.12069	0.15253	0.42323	0.80628
10	1.12103	0.15198	0.42323	0.79707
16	1.12106	0.15192	0.42323	0.78475
20	1.12106	0.15192	0.42323	0.78336
25	1.12106	0.15192	0.42323	0.78336
30	1.12106	0.15192	0.42323	0.78336
35	1.12106	0.15192	0.42323	0.78336

Table 2
Skin friction coefficient $\frac{1}{2}\mathrm{Re}_x^{0.5}C_{f_x}$ and $\frac{1}{2}\mathrm{Re}_x^{0.5}C_{f_y}$ when $\Pr = 1.2, N_b = 0.5, N_t = 0.2, \gamma = 0.1, \delta_e = 0.2, Sc = 1.2$ and $\delta_c = 0.2$.

Parameters (fixed values)	Parameters		$-\frac{1}{2}\mathrm{Re}_x^{0.5}C_{f_x}$	$-\frac{1}{2}\mathrm{Re}_x^{0.5}C_{f_y}$
$\delta = 0.2$	α	0.1	1.47980	0.17619
		0.2	2.01272	0.19923
		0.3	2.68852	0.20252
$\alpha = 0.1$	δ	0.1	1.42483	0.07529
		0.2	1.47980	0.17619
		0.5	1.65094	0.63171

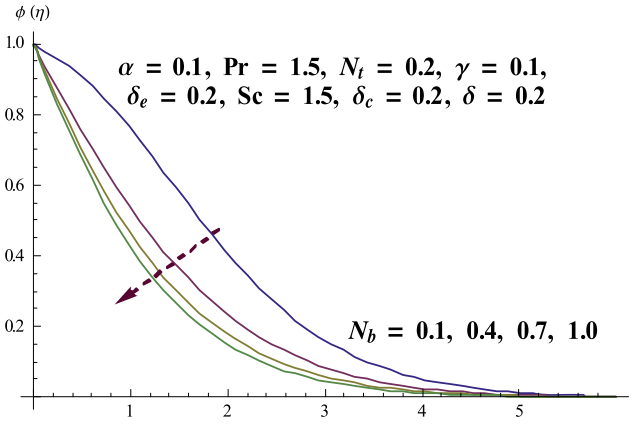

Fig. 13. Behavior of N_b on $\phi(\eta)$.

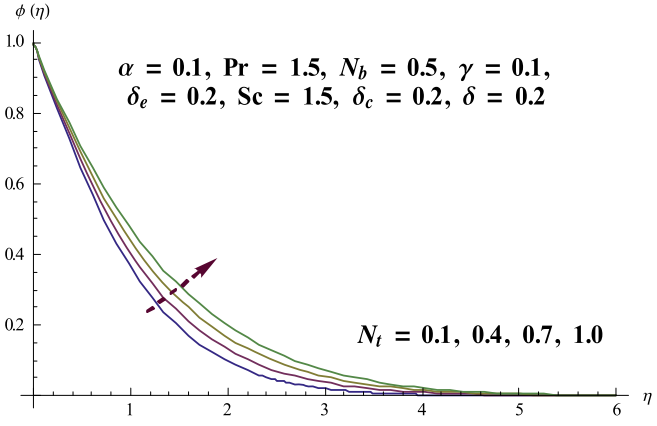

Fig. 14. Behavior of N_t on $\phi(\eta)$.

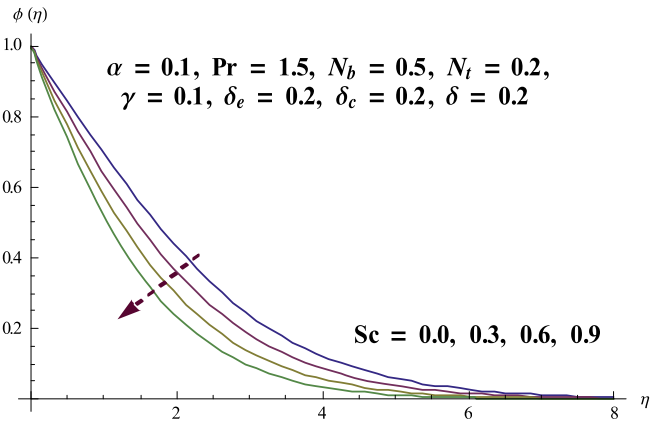

Fig. 15. Behavior of Sc on $\phi(\eta)$.

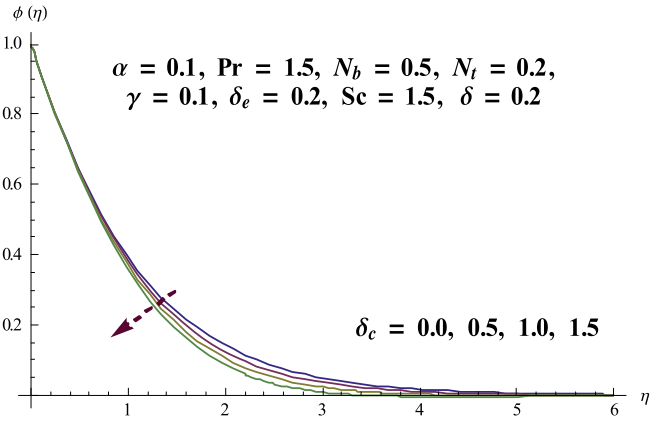

Fig. 16. Behavior of δ_c on $\phi(\eta)$.

of physical variables. Skin friction coefficients are enhanced for α and δ.

Concluding remarks

Three-dimensional flow of viscoelastic nanofluid in view of Cattaneo-Christov double-diffusion theory has been considered. Key points are listed below:

- Velocities $f'(\eta)$ and $g'(\eta)$ are similar in a qualitative sense within the frame of viscoelastic parameter α.
- Temperature via N_b and N_t has similar qualitative effect.
- Reduction in concentration is observed for δ_c.
- The velocities $f'(\eta)$ and $g'(\eta)$ have opposite behavior for larger δ while skin friction coefficient along x- and y-directions are enhanced.
- An increase in N_b gives a reduction in the concentration while it enhances due to N_t.
- Both components of skin friction coefficient are increased via ratio parameter δ.

References

[1] Choi SUS. Enhancing thermal conductivity of fluids with nanoparticle. In: Siginer DA, Wang HP, editors. developments and applications of non-Newtonian flows, MD-vol. 231/FED-vol. 66. New York: ASME; 1995. p. 99–105.
[2] Pak BC, Cho YI. Hydrodynamic and heat transfer study of dispersed fluids with submicron metallic oxide particles. Exp Heat Transf 1998;11:151–70.
[3] Ding Y, Alias H, Wen D, Williams RA. Heat transfer of aqueous suspensions of carbon nanotubes (CNT nanofluids). Int J Heat Mass Transfer 2006;49:240–50.
[4] Duangthongsuk W, Wongwises S. An experimental study on the heat transfer performance and pressure drop of TiO_2-water nanofluids flowing under a turbulent flow regime. Int J Heat Mass Transfer 2010;53:334–44.
[5] Yu W, Xie H, Li Y, Chen L, Wang Q. Experimental investigation on the heat transfer properties of Al_2O_3 nanofluids using the mixture of ethylene glycol and water as base fluid. Powder Technol 2012;230:14–9.
[6] Ayub S, Hayat T, Asghar S, Ahmad B. Thermal radiation impact in mixed convective peristaltic flow of third grade nanofluid. Res Phys 2017;7:3687–95.
[7] Sheikholeslami M, Hayat T, Alsaedi A. MHD free convection of Al_2O_3-water nanofluid considering thermal radiation: A numerical study. Int J Heat Mass Transfer 2016;96:513–24.
[8] Hayat T, Hussain Z, Alsaedi A, Mustafa M. Nanofluid flow through a porous space with convective condition and heterogeneous-homogeneous reactions. J Taiwan Inst Chem Eng 2017;70:119–26.
[9] Hayat T, Ullah I, Alsaedi A, Waqas M, Ahmad B. Three-dimensional mixed convection flow of Sisko nanoliquid. Int J Mech Sci 2017;133:273–82.
[10] Hayat T, Qayyum S, Alsaedi A, Shafiq A. Inclined magnetic field and heat source/sink aspects in flow of nanofluid with nonlinear thermal radiation. Int J Heat Mass Transfer 2016;103:99–107.
[11] Buongiorno J. Convective transport in nanofluids. J Heat Transfer Trans ASME 2006;128:240–50.
[12] Farooq U, Hayat T, Alsaedi A, Liao S. Heat and mass transfer of two-layer flows of third-grade nanofluids in a vertical channel. Appl Math Comput 2014;242:528–40.
[13] Krishnamurthy MR, Prasannakumara BC, Gireesha BJ, Gorla RSR. Effect of chemical reaction on MHD boundary layer flow and melting heat transfer of Williamson nanofluid in porous medium. Eng Sci Tech Int J 2016;19:53–61.
[14] Hayat T, Qayyum S, Alsaedi A, Shehzad SA. Nonlinear thermal radiation aspects in stagnation point flow of tangent hyperbolic nanofluid with double diffusive convection. J Mol Liq 2016;223:969–78.
[15] Zhu J, Yang D, Zheng L, Zhang X. Effects of second order velocity slip and nanoparticles migration on flow of Buongiorno nanofluid. Appl Math Lett 2016;52:183–91.
[16] Gireesha BJ, Mahanthesh B, Shivakumara IS, Eshwarappa KM. Melting heat transfer in boundary layer stagnation-point flow of nanofluid toward a stretching sheet with induced magnetic field. Eng Sci Tech Int J 2016;19:313–21.
[17] Hayat T, Waqas M, Shehzad SA, Alsaedi A. Mixed convection flow of a Burgers nanofluid in the presence of stratifications and heat generation/absorption. Eur Phys J Plus 2016;131:253.
[18] Hayat T, Qayyum S, Waqas M, Alsaedi A. Thermally radiative stagnation point flow of Maxwell nanofluid due to unsteady convectively heated stretched surface. J Mol Liq 2016;224:801–10.
[19] Cattaneo C. Sulla conduzione del calore. Atti Semin. Mat. Fis. Univ. Modena Reggio Emilia 1948;3:83–101.
[20] Christov CI. On frame indifferent formulation of the Maxwell-Cattaneo model of finite-speed heat conduction. Mech Res Commun 2009;36:481–6.
[21] Tibullo V, Zampoli V. A uniqueness result for the Cattaneo-Christov heat conduction model applied to incompressible fluids. Mech Res Commun 2011;38:77–99.
[22] Haddad SAM. Thermal instability in Brinkman porous media with Cattaneo-Christov heat flux. Int J Heat Mass Transfer 2014;68:659–68.
[23] Li J, Zheng L, Liu L. MHD viscoelastic flow and heat transfer over a vertical stretching sheet with Cattaneo-Christov heat flux effects. J Mol Liq 2016;221:19–25.
[24] Hayat T, Qayyum S, Shehzad SA, Alsaedi A. Cattaneo-Christov double-diffusion model for flow of Jeffrey fluid. J Braz Soc Mech Sci Eng 2017. https://doi.org/10.1007/s40430-017-0793-x.
[25] Waqas M, Hayat T, Farooq M, Shehzad SA, Alsaedi A. Cattaneo-Christov heat flux model for flow of variable thermal conductivity generalized Burgers fluid. J Mol Liq 2016;220:642–8.
[26] Shehzad SA, Abbasi FM, Hayat T, Alsaedi A. Cattaneo-Christov heat flux model for Darcy-Forchheimer flow of an Oldroyd-B fluid with variable conductivity and non-linear convection. J Mol Liq 2016;224:274–8.
[27] Sui J, Zheng L, Zhang X. Boundary layer heat and mass transfer with Cattaneo-Christov double-diffusion in upper-convected Maxwell nanofluid past a stretching sheet with slip velocity. Int J Therm Sci 2016;104:461–8.
[28] Hayat T, Muhammad K, Farooq M, Alsaedi A. Squeezed flow subject to Cattaneo-Christov heat flux and rotating frame. J Mol Liq 2016;220:216–22.
[29] Liao SJ. Beyond perturbation: introduction to homotopy analysis method. Boca Raton: Chapman and Hall, CRC Press; 2003.
[30] Ziabakhsh Z, Domairry G, Barnia H. Analytical solution of non-Newtonian micropolar fluid flow with uniform suction/blowing and heat generation. J Taiwan Inst Chem Eng 2009;40:443–51.
[31] Hayat T, Qayyum S, Shehzad SA, Alsaedi A. Simultaneous effects of heat generation/absorption and thermal radiation in magnetohydrodynamics (MHD) flow of Maxwell nanofluid towards a stretched surface. Res Phys 2017;7:562–73.
[32] Farooq U, Zhao YL, Hayat T, Alsaedi A, Liao SJ. Application of the HAM-based mathematica package BVPh 2.0 on MHD Falkner-Skan flow of nanoflui. Comp. Fluid 2015;111:69–75.
[33] Zhao Y, Lin Z, Liu Z, Liao S. The improved homotopy analysis method for the Thomas-Fermi equation. Appl Math Comput 2012;218:8363–9.
[34] Hayat T, Qayyum S, Alsaedi A, Waqas M. Radiative flow of tangent hyperbolic fluid with convective conditions and chemical reaction. Eur Phys J Plus 2016;131:422.
[35] Turkyilmazoglu M. Solution of the Thomas-Fermi equation with a convergent approach. Commun Nonlinear Sci Numer Simul 2012;17:4097–103.
[36] Rashidi MM, Ali M, Freidoonimehr N, Rostami B, Hossian A. Mixed convection heat transfer for viscoelastic fluid flow over a porous wedge with thermal radiation. Adv Mech Eng 2014;204:735939.
[37] Hayat T, Qayyum S, Alsaedi A, Ahmad B. Magnetohydrodynamic (MHD) nonlinear convective flow of Walters-B nanofluid over a nonlinear stretching sheet with variable thickness. Int J Heat Mass Transfer 2017;110:506–14.
[38] Hayat T, Mustafa M, Asghar S. Unsteady flow with heat and mass transfer of a third grade fluid over a stretching surface in the presence of chemical reaction. Nonlinear Analysis Real World Appl 2010;11:3186–97.
[39] Hayat T, Shehzad SA, Qasim M, Obaidat S. Radiative flow of Jeffery fluid in a porous medium with power law heat flux and heat source. Nucl Eng Des 2012;243:15–9.
[40] Khan M, Maqbool K, Hayat T. Influence of Hall current on the f lows of a generalized Oldroyd-B f luid in a porous space. Acta Mech 2006;184:1–13.
[41] Hayat T, Qasim M, Mesloub S. MHD flow and heat transfer over permeable stretching sheet with slip conditions. Int J Numer Meth Fluids 2011;66:963–75.
[42] Hayat T, Ahmed N, Sajid M, Asghar S. On the MHD flow of a second grade fluid in a porous channel. Comput Math Appl 2007;54:407–14.
[43] Qayyum S, Hayat T, Shehzad SA, Alsaedi A. Nonlinear convective flow of Powell-Erying magneto nanofluid with Newtonian heating. Res Phys 2017;7:2933–40.
[44] Qayyum S, Hayat T, Alsaedi A, Ahmad B. Magnetohydrodynamic (MHD) nonlinear convective flow of Jeffrey nanofluid over a nonlinear stretching surface with variable thickness and chemical reaction. Int J Mech Sci 2017;134:306–14.
[45] Shafiq A, Hammouch Z, Sindhu TN. Bioconvective MHD flow of tangent hyperbolic nanofluid with newtonian heating. Int J Mech Sci 2017;133:759–66.
[46] Qayyum S, Hayat T, Shehzad SA, Alsaedi A. Mixed convection and heat generation/absorption aspects in MHD flow of tangent-hyperbolic nanoliquid with Newtonian heat/mass transfer. Rad Phys Chem 2018;144:396–404.